Ann. Geophys., 27, 3577–3590, 2009
www.ann-geophys.net/27/3577/2009/

Annales Geophysicae

Plasma transport in the magnetotail lobes

S. Haaland[1,2], B. Lybekk[3], K. Svenes[4], A. Pedersen[3], M. Förster[5], H. Vaith[6], and R. Torbert[6]

[1]Max-Planck Institute for Solar Systems, Germany
[2]Department of Physics and Technology, University of Bergen, Norway
[3]Department of Physics, University of Oslo, Norway
[4]Norwegian Defence Research Establishment, Norway
[5]Helmholtz Centre Potsdam, GFZ German Research Centre for Geosciences, Germany
[6]University of New Hamshire, NH, USA

Received: 21 January 2009 – Revised: 3 September 2009 – Accepted: 7 September 2009 – Published: 28 September 2009

Abstract. The Earth's magnetosphere is populated by particles originating from the solar wind and the terrestrial ionosphere. A substantial fraction of the plasma from these sources are convected through the magnetotail lobes. In this paper, we present a statistical study of convective plasma transport through the Earth's magnetotail lobes for various geomagnetic conditions. The results are based on a combination of density measurements from the Electric Field and Waves Experiment (EFW) and convection velocities from the Electron Drift Instrument (EDI) on board the Cluster spacecraft. The results show that variations in the plasma flow is primarily attributed to changes in the convection velocity, whereas the plasma density remains fairly constant and shows little correlation with geomagnetic activity. During disturbed conditions there is also an increased abundance of heavier ions, which combined with enhanced convection, cause an accentuation of the mass flow. The convective transport is much slower than the field aligned transport. A substantial amount of plasma therefore escape downtail without ever reaching the central plasma sheet.

Keywords. Ionosphere (Plasma convection) – Magnetospheric physics (Solar wind interactions with unmagnetized bodies; Instruments and techniques)

1 Introduction

The magnetotail lobes are bounded by the central plasma sheet and its boundary layers on one side, and the magnetopause with its adjacent boundary layer, often referred to as the plasma mantle (Rosenbauer et al., 1975), on the other side. The plasma mantle covers much of the high-latitude magnetosphere, extending poleward of the cusp regions and is populated with cold ($\simeq$100 eV), de-energized magnetosheath plasma with typical densities from 0.01–1 cm^{-3}, and tailward flow velocities in the range 100–200 $\mathrm{km\,s}^{-1}$. Similarly, the plasma sheet boundary layer (PSBL), consists of hot plasma with a density around 0.1–2 cm^{-3}. The lobes are characterized by a very low particle density, typically below 0.1 particles per cm^{-3} (e.g., Gosling et al., 1985; Svenes et al., 2008), and a strong and steady magnetic field. Typical magnetic field values range from approximately 30–50 nT, somewhat dependent on geomagnetic activity (e.g., Caan et al., 1975). Tailward of approximately 10 R_E, the magnetic field lines in the northern (southern) central lobe are almost parallel (anti parallel) to the $X_{\mathrm{GSE/GSM}}$ direction.

The magnetosphere is a very dynamical system primarily controlled by the solar wind and the interplanetary magnetic field (IMF). When the IMF has a southward component, it can reconnect with the Earth's geomagnetic field on the dayside magnetopause, and allow plasma from the solar wind and magnetosheath to penetrate into the magnetosphere. The recently opened magnetic field lines are dragged by the solar wind across the polar caps into the magnetotail lobes and then into the central plasma sheet of the magnetotail, where the field lines eventually reconnect and return towards the Earth (Dungey, 1961).

The location of the dayside reconnection line and the region of plasma entry into the magnetotail are also modulated by the IMF B_y component. In the Northern Hemisphere a positive (negative) B_y will cause a displacement of the reconnection region so that the newly opened flux tubes are transported towards dawn (dusk), and oppositely for the Southern Hemisphere (e.g., Cowley et al., 1991). This B_y influence is also reflected in the convection in the lobes (Gosling et al., 1984, 1985; Noda et al., 2003; Haaland et al., 2008), the ecliptic plane (Baumjohann and Haerendel, 1985; Baumjohann et al., 1985, 1986; Maynard et al., 1990; Matsui et al., 2005), and in the polar cap ionosphere (Ruohoniemi and Baker, 1998; Förster et al., 2007; Haaland et al., 2007). In the

Correspondence to: S. Haaland
(stein.haaland@ift.uib.no)

case of northward IMF, reconnection can take place between the IMF and already open polar cap field lines at high latitudes. In such cases, the polarity of the IMF B_x component also plays a role. A positive IMF B_x favours lobe reconnection in the Southern Hemisphere, whereas a negative IMF B_x favours lobe reconnection in the Northern Hemisphere (Crooker, 1986). However, it is still debated how effective a northward directed IMF is in bringing plasma into the central plasma sheet (Sandholt et al., 1999; Imber et al., 2006, 2007; Taylor et al., 2008; Øieroset et al., 2008).

There are also other mechanisms for plasma entry into the magnetosphere, for example diffusion (e.g., Treumann et al., 1995) or overturning of Kelvin-Helmholtz waves along the magnetopause flank (e.g., Hasegawa et al., 2004, and references therein). To our knowledge, no quantitative assessment of the contribution to the lobe density from these sources exist, though.

Another important (and sometimes probably dominant) source of plasma is outflow from the terrestrial ionosphere (e.g., Chappell et al., 1987; Yau and Andre, 1997). Ions are accelerated upward by the electric field arising from charge separation set up by escaping photoelectrons. Ionospheric outflow is thus modulated by solar irradiance. There are actually several important outflow regions in the ionosphere; the polar wind, the ion cleft and the auroral region. Axford (1968) studied theoretical aspects of outflow of light ions (they mainly focused on escape of He^3 and He^4) from the polar cap regions ($\geq 75^\circ$ magnetic latitude), and suggested the term "polar wind" to describe the outflow. Lockwood et al. (1985b) presented a statistical study of O^+ outflow from the dayside ionosphere near the polar cap boundary. This outflow, often associated with outflow of lighter ions, was found to be dependent on both season and geomagnetic activity level. This source is sometimes known as the cleft ion fountain (Lockwood et al., 1985a). A third major source of outflow is the auroral region. The ionization is here mainly caused by precipitating particles. However, since the auroral region is magnetically connected to the near Earth plasma sheet, this source is less relevant as a plasma source for the magnetotail lobes.

A comprehensive survey of the various sources, as well as a quantitative assessment of the relative contribution from each of these sources are given in Huddleston et al. (2005). Solar wind control of outflow rates are discussed in e.g., Cully et al. (2003) and Lennartsson et al. (2004), and the role of particle precipitation and heating is discussed in e.g., Strangeway et al. (2000, 2005).

In this paper we focus on mass transport through the lobes, using measurmenents of convection and plasma density. The low particle density of the magnetotail lobes makes direct measurements with plasma instruments difficult. In addition to the low count rates, measurements are often severely affected by spacecraft charging. A spacecraft immersed in a thin plasma will be charged to large positive potentials. As a result, a part of the low energy particle population will be shielded from the detectors. Moment calculations will therefore not be very reliable. Most of the in-situ information from the magnetotail lobes have been based on magnetic field instruments and measurements from double probe instruments (see e.g., Engwall et al., 2006, and references therein)

The Cluster spacecraft quartet, with its comprehensive set of instruments combined with newly developed techniques have provided new possibilities to obtain more accurate measurements of plasma convection and density in low density region of the Earth's magnetosphere. In this paper, we present estimates of the convective mass transport through the lobes for various geomagnetic conditions. The results are based on convection velocity measurements from the Electron Drift Instrument (EDI), combined with electron density measurements obtained from the Electric Field and Wave Experiment (EFW). The two data sets consist of data collected over a period of 7 years from the Cluster mission, and are very similar to the data sets described in Haaland et al. (2008) and Svenes et al. (2008), respectively.

The rest of this paper is organized as follows: in Sect. 2, we give a description of the EDI and EFW instruments and their data products, as well as an overview of auxiliary data used to establish solar wind conditions and the geomagnetic activity level. Section 3 describes the method to combine the velocity and density measurements. Section 4 contains a statistical overview and a discussion of the results. Section 5 summarizes the paper.

2 Data and instrumentation

The results presented here are mainly based on in-situ measurements from the Cluster quartet of spacecraft. Cluster is a four-spacecraft mission flying in a nearly 90° inclination elliptical polar orbit, with perigee at around 4 R_E and apogee around 20 R_E geocentric distance, and an orbital period of approximately 57 h. The Cluster apogee has moved to the south over the 7 years of data collection reported here. This has resulted in a more extensive coverage of the southern lobe. The instrumentation is identical on all spacecraft, but not all instruments work on all spacecraft. In the science community, the four spacecraft are referred to as SC1, SC2, SC3 and SC4, and we use this notation to distinguish between the different spacecraft here. More details about the Cluster mission and its comprehensive instrumentation can be found in Escoubet et al. (1997).

In addition, measurements of the solar wind, IMF and solar irradiation as well as geomagnetic indices have been used to check correlations, and as inputs to the magnetic field model used for mapping. The data sets and instrumentation are described in some detail in Haaland et al. (2008) and Svenes et al. (2008). For convenience, we here repeat some of this information, and point out some updates and changes in the data bases.

2.1 Plasma convection velocity from the EDI

Measurements of the plasma convection (or drift) velocity were obtained with the Cluster Electron Drift Instrument (EDI). The basis of the electron-drift technique is the injection of two weak monoenergetic electron beams and the detection of the beams after one or more gyrations in the ambient magnetic field. Due to their cycloidal motion, the electron beam can only return to the associated detectors when fired in directions uniquely determined by the magnitude and direction of the plasma drift velocity. Successful operation therefore requires continuous tracking of those directions. The drift velocity is computed either from the direction of the beams (via triangulation) or from the difference in the times-of-flight between the two beams. More information about the EDI technique, hardware, operation, and data analysis can be found in Paschmann et al. (1997); Quinn et al. (2001); Paschmann et al. (2001).

Unlike classical double probe instruments, EDI can measure the entire drift velocity vector, which for a given magnetic field is equivalent to the transverse electric field when gradient drift effects are small. The electric field from EDI thus includes any component along the spacecraft spin axis, but only perpendicular to the magnetic field. The Electric Field and Wave Experiment (EFW), which is based on the double-probe technique, measures the electric field in the spin-plane, which may contain a parallel electric field component. An important advantage of EDI for high-latitude convection measurements is its immunity from wake effects that can interfere with electric field measurements by the double-probe measurements under conditions of low plasma temperature.

EDI does not have a fixed time resolution, and data have been processed down to one second resolution. In this paper, we focus on convection, which is a rather slow process, and we have therefore used 1-min averages. EDI measurements are available for Cluster SC1 and SC3 throughout the entire period covered by this paper, and until April 2004 for SC2. No EDI measurements are available from SC4.

The suitability of EDI for measurements in the polar cap region and the magnetotail lobes has been demonstrated in publications by e.g., Noda et al. (2003), Haaland et al. (2007, 2008) and Förster et al. (2007, 2008). The large, relatively stable magnetic fields typically encountered by Cluster over the polar caps and in the lobes are regimes in which the EDI technique provides high accuracy with its geometric measurement technique.

Since there are no parallel electric fields in this region of space, the EDI measurements can be mapped from one region of space to another (e.g., Maynard et al., 1995; Hesse et al., 1997). This requires steady state conditions and an accurate model of the magnetic field, in this case the Tsyganenko T02 model (Tsyganenko, 2002a,b, including the latest updates to the code, dated April 2008). We can therefore utilize all EDI measurements along field lines threading the lobes, including measurements from sunward of the terminator. Details of the mapping procedure are given in (Haaland et al., 2008).

The EDI data set consists of approximately 320 000 one minute averages, each record containing the velocity measurement from EDI as well as auxiliary data such as spacecraft position, geomagnetic indices and solar wind information.

2.2 Plasma density from EFW probes

Each Cluster spacecraft also has an electric field experiment based on the double probe technique. Four spherical probes and preamplifiers are located at the tips of four radial wire booms which spin with the spacecraft at 0.25 Hz. The two probe pairs have a baseline of 88 m and this allows for measuring two orthogonal electric field components in the spin plane. The EFW experiment has been described by Gustafsson et al. (1997) and Pedersen et al. (1998). Comparisons between EFW and EDI have been published by Eriksson et al. (2006).

A conductive surface, like a satellite, immersed in a plasma will attain a potential relative to the surrounding plasma such that the sum of currents to it becomes zero. In a tenuous lobe plasma the available photoelectron emission current from sunlit spacecraft surfaces exceeds the current from collected ambient electrons. A current equilibrium can only be achieved by a positive spacecraft where most emitted photoelectrons orbit back to the spacecraft and a small fraction escape in balance with collected electrons. A reduction of ambient electrons will result in a more positive spacecraft required for further reduction of escaping photoelectrons. The equilibrium situation will be attained essentially instantaneously in a particular environment, but the vehicle potential may change as a function of time as the spacecraft moves through various regions of space. Electrons emitted from EDI may influence this equilibrium. The Active Spacecraft Potential Control (ASPOC – see Torkar et al., 2001) instrument in normal mode emits a 10 μA ion current that changes the spacecraft current equilibrium.

In a tenuous plasma Cluster will acquire a large positive potential of the order 30–50 V. When the magnetic field vector has a small angle with the spin plane, and ions have a drift parallel to the magnetic field, an ion wake with a negative charge will be set up by the large potential around the spacecraft and act as a hindrance to the parallel ion drift. A sufficiently large parallel ion drift will therefore upset electric field measurements. In this paper we do not utilize the electric field measurements from EFW, but use the probes to determine the spacecraft potential that is a function of the ambient plasma density.

If active experiments are not running, a satellite in the tenuous lobe plasma region will typically attain an equilibrium potential where collected ambient electrons and escaping photo-electrons are balanced. In this plasma, currents

due to ions are negligible in comparison. With knowledge of the photo-electron escape current as a function of spacecraft potential it is then possible to estimate the electron density leading to the equilibrium current. Solar radiation in the Extreme Ultraviolet (EUV) range are required to generate photo-electrons with enough energy to escape a satellite at these large positive potential values. Solar cycle variations of EUV radiation must therefore be taken into account.

In the magnetotail lobes, the potential attained by the spacecraft will consequently be so high that it prevents a large part of the ion distribution from reaching the ion sensors. Ion moments, including density measurements, from these sensors will therefore be incorrect. The electron spectra on the other hand may be contaminated by photoelectrons. Even active sounder techniques are often inaccurate in this environment due to low plasma density and high photoelectron flux. However, since the spacecraft potential will be a function of the properties of the surrounding plasma a proper calibration of the spacecraft potential measurements will yield good estimates of the ambient plasma density with a high time resolution.

The potential distribution around Cluster in a tenuous plasma has been modeled by Cully et al. (2007), who showed that plasma potential near the probes, located 44 m from the spacecraft, is approximately 20% of the spacecraft potential relative to the ambient plasma potential. By establishing a functional dependence between the spacecraft potential and the ambient plasma density through a thorough calibration program, the spacecraft potential measurements may then be routinely converted to density measurements. A detailed explanation of this calibration procedure is given in Pedersen et al. (2008), but basically, the relationship between the potential and plasma density is given by the equation:

$$n_e = Ae^{-V_{SP}/B} + Ce^{-V_{SP}/D} \quad (1)$$

where V_{SP} is the potential difference between the spacecraft and the probes, and as such represent the direct measurements. The factors A, B, C and D are empirically determined coefficients that vary over the solar cycle. The above formula is valid for densities up to approximately $0.5\,\mathrm{cm}^{-3}$.

Active instruments such as EDI usually prevent successful EFW density measurements. Most of EFW probe data are taken therefore from SC4, where EDI does not operate, but there are also a significant number of samples from SC2, where EDI ceased to operate in April 2004. There are also a few hours of data from SC1 and SC3. Since the density has to be based on in-situ measurements, we can only utilize data from July to October, when Cluster traverses the nightside magnetotail lobes.

The full EFW data set consists of approximately 476 000 one minute averages, containing the calculated density as well as solar wind and auxiliary parameters as in the EDI data set. In addition, the data set contains plasma moments from the Cluster Ion Spectrometer (CIS – Rème et al., 2001), and the Plasma Electron And Current Experiment (PEACE – Johnstone et al., 1997) used to exclude samples from the central plasma sheet and its boundary layers (see Sect. 4.1).

2.3 Solar wind and auxiliary data

The transport of plasma in the magnetosphere is mainly controlled by the solar wind, in particular the direction of the IMF. The IMF direction is often described in terms of clock angle, i.e., the angle between the Z_{GSM} axis and the projection of IMF into the $\mathrm{YZ}_{\mathrm{GSM}}$ plane. A 0° clock angle indicates a purely northward IMF; 90° indicates an IMF pointing in the $+Y_{\mathrm{GSM}}$ direction and so on. In this study, measurements of the IMF and solar wind plasma data are taken from the OMNI data set provided by CDAWEB (http://cdaweb.gsfc.nasa.gov). This data set contains, among others, IMF, solar wind velocity and proton density properly time shifted to the upstream magnetopause. The time shift of the solar wind measurements in the OMNI data set is done according to the phase front propagation technique, first described in Weimer et al. (2003). The validity of this method has been demonstrated recently by Mailyan et al. (2008); Weimer and King (2008).

Note that there are some subtle differences between the OMNI data set used in the present study and the data set used in Haaland et al. (2008) and Svenes et al. (2008): These studies used IMF data from the Advanced Composition Explorer (ACE) spacecraft only, whereas the OMNI data set contains data from several spacecraft. The OMNI data also has a different procedure to handle data gaps.

2.3.1 Removing periods with unreliable IMF data

Even with a fairly accurate time shift of the solar wind data, there will be time segments when the IMF orientation at the magnetopause is uncertain. This is particularly true for times where the IMF fluctuates rapidly. To avoid ambiguities, we have filtered out such time periods using the so-called bias filtering, introduced by and illustrated in Haaland et al. (2007). To each data record (consisting of time tags, Cluster measurements, solar wind measurements, geomagnetic indices etc.) we assign a so called bias vector which describes the IMF stability. Records with bias vector lengths below a certain threshold are thereafter discarded.

Calculation of this bias vector basically consists of the following steps: First, a set of N one-minute IMF measurements, B_i, projected into the $\mathrm{YZ}_{\mathrm{GSM}}$ plane are normalized. Thereafter, the N vectors are added and an average vector – a bias vector $\boldsymbol{b}=1/N\ \Sigma\ (B_i/|B_i|)$ is calculated. If the N original IMF vectors were parallel, i.e., a perfectly stable IMF direction, the bias vector would have unit length. Correspondingly, if the N vectors had random directions, the length of the resulting bias vector would be zero. The length of the bias vector is thus a measure of IMF directional stability, and its direction is used to determine the average clock angle.

For this study, the bias vector for a record at time t has been calculated from N=30 individual one-minute IMF vectors, starting at $t-10$ min to $t+20$ min. This asymmetric time interval is meant to take into account any residual error in the time shift of the solar wind data as well as additional time to propagate IMF changes to the lobe regions. Records with bias vector lengths less than 0.96 have been filtered out. A similar IMF filtering was also applied in the Haaland et al. (2008) and Svenes et al. (2008) papers.

2.4 Geomagnetic disturbance indices

To study correlations between the mass flow and geomagnetic activity, our data set also contains a set of indices characterizing various processes in the magnetosphere. The D_{st} (Disturbed Storm Time) index is a measure of the horizontal magnetic deflection on the Earth at equatorial latitudes. Negative deflections in D_{st} are mainly controlled by the Earth's ring current and the cross-tail current, though the solar wind pressure also contributes (e.g., Burton et al., 1975; O'Brien and McPherron, 2000). Positive deflections are usually caused by pressure enhancements in the solar wind which cause a displacement of the magnetopause. The D_{st} index was provided in digital form by the World Data Center A (WDCA), Kyoto, and re-sampled and interpolated to one minute time tags of the Cluster data using the method described in Schwartz (1998).

The Auroral Electrojet (AE) index, is a measure of the horizontal magnetic deflection at auroral latitudes. It is supposed to reflect auroral geomagnetic activity, primarily associated with tail magnetic activity. However, the longitudinal coverage is often limited, so localized substorm activity may sometimes escape detection. The AE index was also obtained at one minute resolution from WDCA.

2.5 Information about solar irradiance

As a proxy for solar irradiance, we have used data from the Solar Extreme ultraviolet Experiment (SEE), on board the Thermosphere, Ionosphere, Mesosphere Energetics and Dynamics (TIMED) spacecraft. This sensor tracks the Sun for about 10 min each orbit to measure solar radiation in the 5 to 45 nm range. For convenience, we have interpolated the TIMED data to the 1 min resolution of the rest of the data set. Since the TIMED satellite was launched in late 2001, we only have solar irradiance data from 2002–2007.

2.6 Constraints and limitations of the data sets

The results presented in this paper have been collected over a period of 7 years, spanning from the start of the operative Cluster science mission in February 2001 until late 2007. For several reasons, the data set is not continuous throughout this time period. In the early phase of the Cluster mission, telemetry constraints prevented full data coverage. Both the EDI and EFW instruments are limited by operational constraints. Since EDI is an active experiment emitting an amplitude-modulated electron beam, it interferes with the wave measurements on Cluster. EDI is therefore operated with a duty-cycle that has been negotiated with the other experiments on Cluster. Also, due to the working principle of EFW density estimates, simultaneous measurements of convection from EDI and EFW density measurements are not possible if the sum of the two beam currents of EDI exceeds about 90 nA. Higher beam currents will typically drive the spacecraft potential to values outside the range where density measurements can be done.

In addition to the limitation of data return from Cluster, there are also shorter data gaps in the OMNI solar wind data. Since the solar wind history is an input parameter of the T02 magnetic field model used for mapping, some attention is still needed when there are gaps in the solar wind data: The G1 and G2 factors of the T02 model are based on the preceding 1 h history of the solar wind. If there is a gap within this period, the G1 and G2 factors are simply based on fewer samples.

3 Methodology

The convective mass flow, i.e., the amount of plasma transported through a unit area within a given time can be expressed by:

$$Q = (n_i * m_i + n_e * m_e) * V_\perp \ \left[\frac{kg}{m^2\, s}\right] \tag{2}$$

where n_i and n_e are the ion and electron number densities, and m_i and m_e are the corresponding ion and electron masses. $V_\perp$ is the bulk velocity of the plasma. Due to the mass ratio between electrons and ions (any species), the electrons can be neglected. In a plasma governed by MHD, one can in addition assume quasi-neutrality (n_e=n_i). The above relation can therefore be simplified to:

$$Q = (n_e * m_i) * V_\perp \ \left[\frac{kg}{m^2\, s}\right] \tag{3}$$

With Cluster, both $V_\perp$ and n_e can be measured with a high degree of accuracy with the EDI and EFW instruments, respectively. Note that we can only quantify the mass flow perpendicular to the magnetic field. For transport along the field, we refer to Engwall et al. (2009b), which uses a similar instrumentation to address ionospheric outflow of cold plasma. The ion mass, m_i is not a constant, but depends on the plasma composition, which again depends on the disturbance level (e.g. Comfort and Horwitz, 1981; Lennartsson and Sharp, 1982; Young et al., 1982; Lennartsson, 1994; Vaisberg et al., 1996; Barakat and Schunk, 2006).

In order to obtain the mass flow according to Eq. (3), we obviously need an estimate of the ion mass. Due to the issues with spacecraft charging and low count rates mentioned

above, the mass resolution capabilities of the CIS or RAPID particle instruments on board Cluster cannot help us in this region of extremely thin plasma. Without making any assumptions about plasma composition and ion mass, we can therefore only determine the number flux, i.e., the quantity $Q/m_i = n_e * V_\perp$ from our measurements. In the remainder of this paper, we will therefore primarily discuss number flux.

3.1 Combining the EFW and EDI data sets

Since the derivation of density rely on the spacecraft potential (ref. Eq. 1), a simultaneous measurement of density and velocity is usually not possible. When ASPOC is off, the electron beam emitted during EDI operation artificially alters the spacecraft potential to such a degree that the density determination becomes impossible whenever the total EDI beam current exceeds approximately 90 nA. In the statistical results presented here, we have therefore done the combination in parameter space, i.e., measurements from EDI are combined with EFW measurements taken under similar geomagnetic conditions, and from the same region (i.e., the lobe), but not necessarily sampled simultaneously or from the same spacecraft.

3.2 Accuracy and statistical variations

The uncertainties in our results can roughly be divided into three parts: 1) uncertainties in the measurements, 2) validity of the underlying models or assumptions, and 3) statistical spread.

Experimental uncertainties are probably the smallest error source in our data set. Due to the purely geometric measurement technique of the EDI instrument, the measurement uncertainties are almost negligible for the convection measurements. The density measurements are derived from the spacecraft-probe voltage difference (V_{SP} – see Eq. 1), which can be measured with a fairly high accuracy. Errors in the density are therefore mainly governed by the functional dependence between the potential and ambient plasma density. The uncertainty in the density from EFW can be estimated by comparisons with the CIS, PEACE and WHISPER experiments on Cluster during some favourable conditions (Pedersen et al., 2008). This uncertainty increases from approximately 20% to 30% when the density goes from 1 cm^{-3} to 0.05 cm^{-3}. For lower densities no comparisons with other experiments have been possible, and the uncertainty is probably of the order of 50%.

For the convection and mapping of the EDI measurements, we make two assumptions. First, we assume that the magnetic field lines are equipotentials. To our knowledge, there exists no mechanisms that can set up significant field aligned electric fields above the polar cap or in the lobes where we obtain our EDI samples, so this assumption can be justified. Secondly, the validity of the mapping depends on the quality of the magnetic field model used. For single events, and certain conditions there can be large discrepancies between the observed and modelled magnetic field (e.g., Pulkkinen and Tsyganenko, 1996; Smart and Shea, 2001). However, in a statistical sense, the magnetic field model probably reproduces the geomagnetic field fairly well in this region of space (Woodfield et al., 2007).

The variability in the binned EDI measurements were shown in Fig. 4 of Haaland et al. (2008). For southward directed IMF, which is most important for the mass transport, the statistical variability was found to be low, with a well defined average convection magnitude and direction.

When dealing with statistical studies, it is legitimate to ask whether a mean (i.e., an arithmetic mean of all values) or a median (i.e., the most probable value) best characterize a data set. A look at the distribution of the quantity in question gives some hints here. For a Gaussian distribution, the mean and median are identical, so using one or the other does not make any difference. This is almost the case for our EDI data set; the convection measurements are in the range 0–50 $\mathrm{km\,s}^{-1}$, with an average of around 7.7 $\mathrm{km\,s}^{-1}$ in Z-direction in both hemispheres. This is also close to the maximum of the distribution, so using a mean value is reasonable to characterize the convection.

The EFW density measurements, on the other hand, vary over a large dynamic range, The smallest density is 0.006 cm^{-3}, and the highest (limited by our initial filtering of the data set) is 0.5 cm^{-3}. In addition, the distribution of the measurements is highly non-Gaussian with a high density tail (see Fig. 3 of Svenes et al., 2008). The EFW data set where samples with plasma $\beta \geq 0.01$ have been discarded, has a median of 0.063 cm^{-3}, and a mean value of 0.093 cm^{-3}. About 75% of the samples have a density lower than the arithmetic mean. For the unfiltered data set, the difference between mean and median is even larger. We therefore believe that a median of all measurements gives the best representation of the average lobe density.

Thus, in the following, when we use the term "average", this is obtained from the arithmetic mean of the EDI convection velocity measurements, and median value of the EFW density measurements.

4 Results

Figure 1 shows a graphical representation of the EDI and EFW data sets used for this study. The upper left panel shows a profile of the overall convection velocities mapped into $1\times1\,R_E$ bins in a $\mathrm{YZ_{GSM}}$ plane at X=$-10\,R_E$. Only EDI vectors inside a $20\,R_E$ radius around the X_{GSM} axis are shown. Each arrow shows the average convection direction within that particular bin. Colors indicate the convection velocity in the XY plane (which is essentially $V_\perp$ in the central lobes, since the magnetic field is nearly aligned with the $\pm X_{\mathrm{GSE/GSM}}$ axis here). The averaging and mapping procedure, described in more detail in Haaland et al.

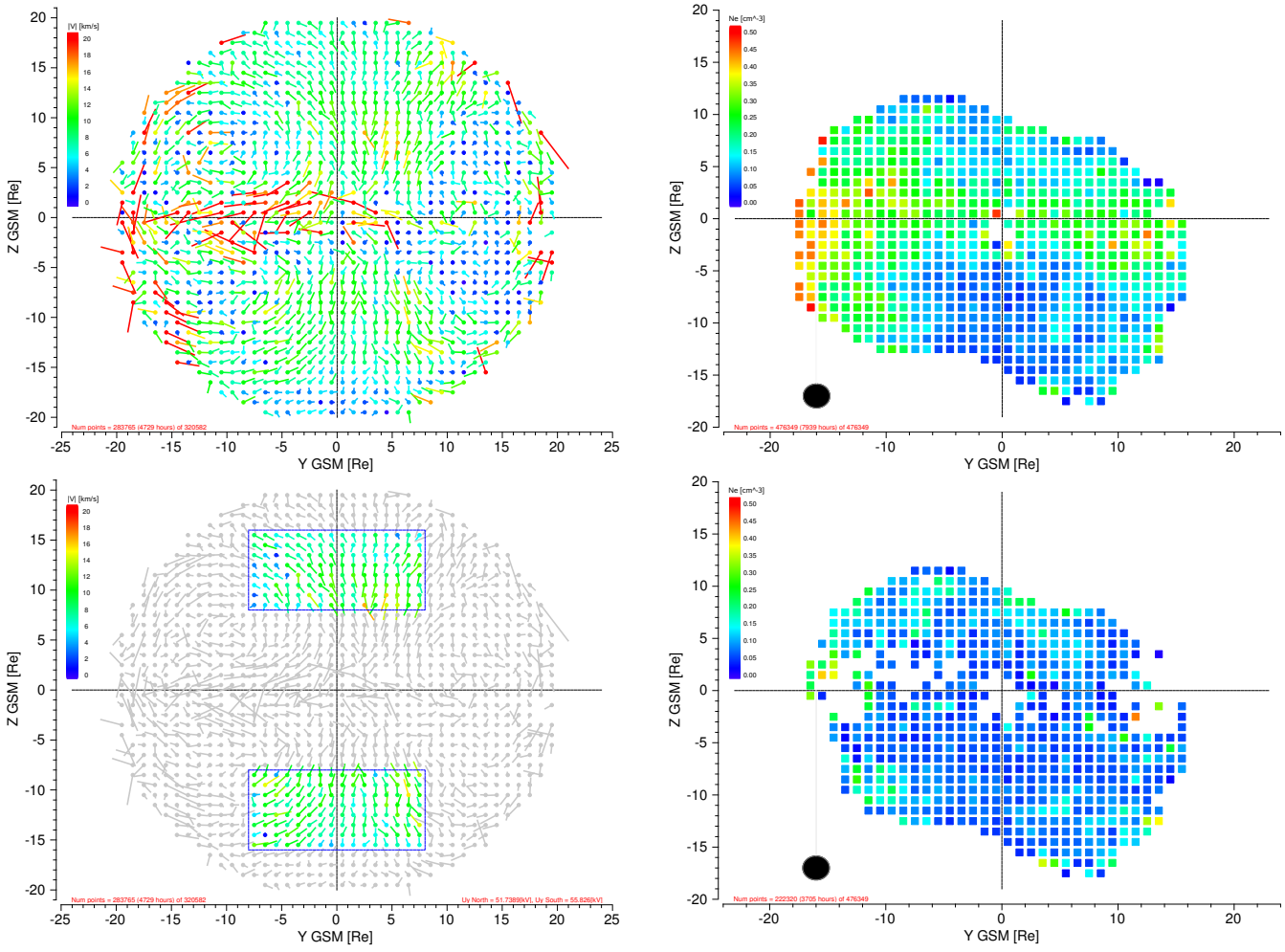

Fig. 1. YZ_{GSM} view of the convection and density. Top left: Average convection for the full data set. The arrows show the convection strength (color coded) and direction of the convection in the ZY_{GSM} plane. Top right: electron density (color coded) for the full set. Bottom: Similar, but only including records we define as lobe (see Sect. 4.1). Convection data are mapped into an YZ plane at X=−10 R_E, whereas the density plots show averages of densities collected between X=−6 R_E to X=−21 R_E.

(2008), implies that all EDI measurements obtained on field lines threading the lobe at X=−10 R_E have been used to calculate the average within that particular bin. During the period February 2001 to October 2007, a total of approximately 320 000 one-minute averages of the convection from EDI were collected. This corresponds to more than 5300 h (of which approximately 4700 h of data map to locations inside the 20 R_E limit in Fig. 1)

The upper right panel illustrates the average densities, also binned into 1×1 R_E bins, but collected between X=−6 R_E and X=−21.1 R_E (maximum Cluster apogee). Approximately 476 000 records of one minute averages (7900 h) of electron density from EFW were collected.

The lower panels of Fig. 1 show the corresponding filtered data set, where only data which we classify as lobe measurements (see Sect. 4.1) are included.

The largest velocities can be found near the central plasma sheet and near the magnetopause flanks (outside the 20 R_E radius shown here, measured convection velocities are even stronger, although mapping to locations close to the magnetopause and magnetosheath is probably not as reliable as mapping to the central lobes). One should have in mind, however, that the magnetic field deviates significantly from the almost sunward/anti-sunward alignments in the lobes. There may therefore be significant convection in the ±X direction, which cannot be determined from the projection into the YZ_{GSM} plane shown in Fig. 1.

As pointed out in Haaland et al. (2008), the large scale vortex-like circulation patterns in these plots are the magnetospheric counterparts of the ionospheric convection cells. Inside the blue boxes which we use to calculate characteristic lobe averages, the convection (and thus the mass flow), is primarily towards the plasma sheet, but there is a significant cross-tail component.

Although there is a seasonal motion of the plasma sheet which smears things out, the central plasma sheet is also clearly discernible from the unfiltered density measurements shown in the upper right panel. The thickening of the plasma sheet towards the flanks (e.g., Baumjohann and Paschmann, 1990; Huang and Frank, 1994; Wing and Newell, 2002) is also apparent from this profile.

4.1 Defining the lobe

In the literature, one can find several methods to classify the lobe. Depending on purpose and available instrumentation, several experimental identifications of the lobes are conceivable. For example, Caan et al. (1975) studied the magnetic pressure enhancements during substorms, and used the magnetic field strength to identify the lobes. Baumjohann et al. (1989) used a combination of spacecraft charging effects and plasma density from the AMPTE/IRM spacecraft to separate lobe samples from the plasma sheet and plasma sheet boundary layers. There are also examples of purely geometric definitions, or a combination of observations and geometry to define the lobe. This is the case for the Haaland et al. (2008) and Svenes et al. (2008) papers which form the basis for the present study.

Whereas the EDI data can be sampled over large regions and mapped into a fixed plane, this is not possible with scalar values like density or plasma β, which have to be sampled locally. Due to these fundamentally different properties of the measurements, we have applied two different definitions of the lobe in the two data sets.

For the EDI dataset, the average convection velocity is obtained by averaging all EDI measurements which, according to the T02 model map into two (northern and southern lobe, respectively) $8\times16\,R_E$ regions in the XY-plane at X=$-10\,R_E$. This approach, illustrated in the lower left panel of Fig. 1 is similar to the definition used in Haaland et al. (2008). Note that this delineation is very conservative to avoid inclusion of measurements from the plasma sheet and the magnetopause and their boundary layers. Still, the two boxes contain 65 000 records (Northern Hemisphere) and 83 000 records respectively, which corresponds to 1083 and 1383 h of data, respectively. Within these boxes, the magnetic field is nearly aligned with the $\pm$X direction, so there is only negligible convection in the X-direction.

The EFW data set is based on in-situ measurements, and the region covered is primarily limited by the spacecraft orbit. For this data set, we have defined the lobe as the region of space traversed by Cluster between X=$-6\,R_E$ to X=$-21.1\,R_E$ and then used the plasma β to exclude the high density regions of the plasma sheet. The β used for this exclusion is derived from the observed CIS-CODIF and PEACE plasma moments combined with FGM magnetic field values. As pointed out above, the plasma moments are not very reliable in the lobe, but still sufficient for our purpose. After some experimenting, we found that a definition of the lobe as a region where $\beta\leq0.01$ gave reasonable results.

Our β filter removes most of the plasma sheet values, and the values in the lower right panel of Fig. 1 are much lower, typically less than $0.1\,\mathrm{cm}^{-3}$ and without any strong gradients. A substantial number of measurements near the central plasma sheet are excluded with the β filtering, but the dataset still contains approximately 222 000 records (3700 h).

With an average convection velocity in the Z-direction of $7.7\,\mathrm{km\,s}^{-1}$ and a most probable number density of 0.063 particles per cm^{-3}, the estimated number flux amounts to $Q/m_i=4.85\times10^8\,\mathrm{s}^{-1}\,\mathrm{m}^{-2}$. The density is lower than the average value of $0.16\,\mathrm{cm}^{-3}$ reported by Engwall et al. (2009b), also based on EFW double probe measurements. However, they did not explicitly attempt to remove plasma sheet measurements (although most plasma sheet were excluded due to the applied measurement technique), and used the geometric mean rather than the median value.

If we assume an average O+ abundance of 50% (based on the average disturbance level and the results of Lennartsson, 1994), we obtain an effective ion mass of $m_i=8.5m_p$. The corresponding mass flow (Eq. 3) then amounts to $Q=7.3\times10^{-18}\,\mathrm{kg\,s}^{-1}\,\mathrm{m}^{-2}$.

4.2 Correlations and dependencies

Next, we investigate how the number flux depends on external inputs such as the solar irradiance, varying solar wind and IMF direction as well as processes internal to the magnetotail, reflected by the disturbance indices AE and D_{st}.

For this purpose, we calculate the averages from subsets of the full data set. The sizes of these subsets are a compromise between adequate resolution and sufficient data coverage. For most of the ranges, the subsets still contain thousands of records, and the statistical uncertainty is negligible. However, for extreme values of some of the driver parameters, the coverage (and thus the statistical confidence) is sometimes poor, and results from these ranges should thus be considered with caution. When interpreting these results, one should also have in mind that some quantities are partly mutually correlated (see e.g., Table 1 in Förster et al., 2007); for example, the effects reflected by the D_{st} and AE indices are ultimately driven by the solar wind.

The results are given in Fig. 2. Since we focus on inflow to the plasma sheet, we only show the Z_{GSM}-component of the velocity and number flux. The left panels show histograms of the convection velocity for different ranges of the driver parameters. The middle panel contains the EFW density for the same subset division, and the right panels show the corresponding calculated number flux Q/m_i. Average convection velocities vary between $\approx$1 and $13\,\mathrm{km\,s}^{-1}$, and the averaged densities are in the range 0.05 to 0.12 cm^{-3}. The resulting number fluxes are in the range 1.5×10^8 to $11\times10^8\,\mathrm{s}^{-1}\,\mathrm{m}^{-2}$.

In the following, each of these dependencies is discussed in some detail.

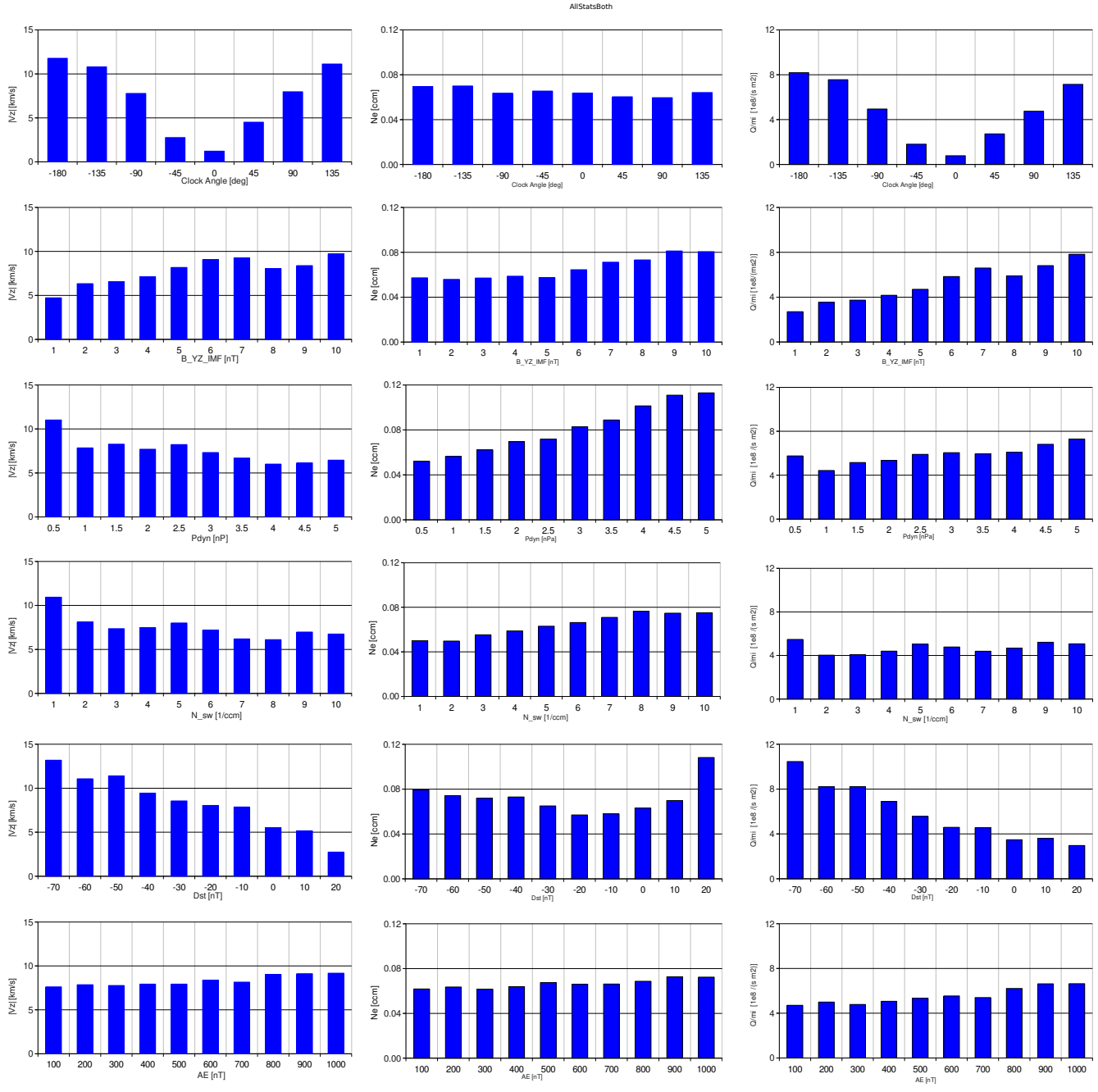

Fig. 2. Correlation between convection, density and number flux versus solar wind and disturbance parameters. The left panels show the average convection velocities, the middle panels show average densities, and the right panels show the calculated number flux for each subset of a particular driver parameter. From top to bottom, we show the correlation of these three parameters versus **(a)** IMF clock angle, **(b)** IMF magnitude, **(c)** solar wind dynamic pressure, **(d)** solar wind density, **(e)** the D_{st} index, **(f)** the AE index. For the clock angle correlation, the numbers along the horizontal axis show the center of the clock angle sector, i.e., 0 means the average obtained from the 45° wide clock angle sector ranging from from −22.5 to +22.5 degrees. For the other parameters, the numbers indicate the upper limit of the range.

4.2.1 Clock angle – IMF direction

As expected the number flux is much stronger for large clock angles (i.e., IMF southward) than for small ones (IMF northward). This is mainly due to the increased convection during such periods. There seems to be little or no correlation between the density and the IMF direction, which is somewhat surprising, as one should expect enhanced transfer of

plasma from the solar wind and magnetosheath during periods with southward IMF. Due to the correlation between IMF and geomagnetic activity, one would also expect higher outflow from the ionosphere during southward IMF. One explanation for the missing correlation may be that loss processes such as field aligned tailward escape of plasma balance any increased input.

4.2.2 IMF magnitude

As already pointed out in Haaland et al. (2008), the convection is positively correlated with IMF magnitude. The density also has a positive correlation, but this is most likely a secondary effect: a strong IMF gives strong convection, thus higher geomagnetic activity and corresponding increased ion outflow from the ionosphere, which is again balanced by increased electron density.

4.2.3 Solar wind density and dynamic pressure

The solar wind dynamic pressure dependence shows a weak but significant anti-correlation with the convection, whereas the lobe density shows a positive correlation with this parameter. One possible explanation here is a compression of the magnetosphere. For the convection correlation, one can imagine that the same amount of flux has to be transported per time unit, but over a shorter distance due to the smaller volume of the magnetosphere. Thus, the velocity decreases with increasing dynamic pressure. For the density, a compressed magnetosphere means that the same amount of particles are distributed over a smaller volume. Unless this is balanced by e.g., enhanced escape downtail, the density will increase. The compression scenario has some support in simulations (e.g., Shue et al., 1997) and observations (e.g. Russell et al., 1999; Wilken et al., 1982, and references therein). Despite the opposite correlation of convection and density, the number flux also shows a positive correlation with dynamic pressure.

Since the dynamic pressure is a function of the solar wind density and the solar wind velocity (and to some extent the composition), it may be useful to try to determine whether the response in the lobes is governed by density or velocity changes in the solar wind. The results show a similar, although less pronounced dependency between lobe density and solar wind density as for the dynamic pressure dependency. The convection and the resulting mass flux, on the other hand, do not seem to be significantly influenced by either solar wind density or solar wind flow velocity, however.

4.2.4 D_{st} dependence

Both convection, density and thus the calculated number flux show a correlation with the D_{st} index. The D_{st} index, which is primarily a measure of the ring current strength, is mainly driven by enhanced dayside reconnection, which again enhances the convection. Lower values of D_{st} means a stronger ring current and typically more geomagnetic disturbance and higher ionospheric outflow (e.g., Huddleston et al., 2005). Positive values of D_{st} are sometimes associated with compression of the magnetosphere. The positive correlation between density and D_{st} values above -10 nT may reflect this.

4.2.5 AE dependence

The AE index shows a much weaker dependence than the D_{st} correlation for both velocity and density. One should have in mind that AE index primarily reflects fairly short-lived and localized processes, such as substorms and bursty bulk flow events typically combined with auroral activity. The flow shear associated with these processes will typically set up field aligned currents which are closed in the auroral zone ionosphere and thus causes the perturbation of the magnetic field which again changes the AE index. The D_{st} index, on the other hand, mainly reflects large scale geomagnetic storm time scales (typically several days from initial phase to recovery).

Since the auroral region mostly maps to the near Earth plasma sheet, we do not expect any direct response in the lobe density as a result of enhanced ionospheric outflow from the auroral region. Parallel electric fields associated with auroral activity means that the ion outflow is of a more energetic nature, and the residence time in the lobe is low for these ions.

4.2.6 Solar irradiance

In addition to the correlations shown in Fig. 2, we also checked the dependence on solar irradiation, represented by measurements of solar extreme ultraviolet flux from the TIMED spacecraft (see Sect. 2.5). In Svenes et al. (2008) a positive correlation was reported for density values above $0.2\,\mathrm{cm}^{-3}$. Since the majority of our density measurements are below $0.2\,\mathrm{cm}^{-3}$, however, we do not find a strong correlation when we include the full data set.

5 Summary and discussion

Based on about 4700 h of convection data and 3700 h of electron density data, we have investigated the number flux through the Earth's magnetotail lobes for various geomagnetic conditions. To obtain these two data sets, we have applied very conservative selection criteria to ensure the best possible data quality. All records where the upstream IMF conditions were doubtful, either due to rapid variations or due to uncertain time shift of the IMF information from the solar wind monitor, have been discarded. EDI data, which due to its purely geometric measurement technique are very exact, have been mapped to the lobes using the T02 magnetic field model, parameterized with the prevailing IMF and solar wind conditions. To overcome limitations and inaccuracies in plasma moments, we also utilized a very conservative

plasma β threshold to make sure only densities from the lobes are included in the data set.

The average convection velocity in the Z_{GSM} direction is $7.7\,km\,s^{-1}$, and the most probable density is $0.063\,cm^{-3}$. The convective velocity is thus much lower than the field aligned velocity of around $28\,km\,s^{-1}$reported by (Engwall et al., 2009a,b). It is therefore reasonable to assume that a substantial amount of plasma escape downtail along open field lines without ever reaching the plasma sheet.

Most of the variation in the number flux and thus mass transport seem to stem from changes in the convection speed. With some exceptions, the density seem to be less dependent on external drivers like the IMF, or secondary effects reflected by the AE and D_{st} disturbance indices.

The only external parameter that seems to significantly influence the lobe density is the solar wind dynamic pressure. However, the correlation seen is most likely the result of a compression of the whole magnetosphere rather than an explicit increase of total plasma content. Our data does not provide support for enhanced plasma transfer as a result of higher solar wind dynamic pressure or higher solar wind density.

The fact that the IMF clock angle does not seem to have a major influence on the density is interesting. A southward IMF greatly enhances the reconnection on the dayside magnetopause, and thus in theory enhanced entry of magnetosheath plasma into the magnetosphere. On a statistical basis, however, this does not seem to be reflected in the lobes. This may suggest that variations in the overall ion density is largely controlled by outflow from the ionosphere.

Since we are unable to determine the ion composition, we are also unable to quantitatively discuss the mass density and mass flow. However, as pointed out in Sect. 3, the oxygen abundance and thus the average ion mass increases with increasing disturbance level. Due to the large mass ratio between protons and oxygen, even small increases in the oxygen abundance cause significant changes in the mass flow. The ion composition also plays an important role for fundamental plasma properties such as e.g., the Alfven speed, as well as threshold levels for many plasma instabilities and wave modes.

As seen from Fig. 2, the difference between the minimum number flux conditions occurring during northward IMF and the maximum conditions occurring at low D_{st}-values is about one order of magnitude. Furthermore, even the difference between the number flux at strong and medium D_{st}-conditions is at least a factor of two. This implies that most of the mass flow toward the plasma sheet occurs during those periods which are characterized by very strong geomagnetic activity. In turn, this implies that due to this mass loading process the stability of the plasma sheet at any one particular time will be very difficult to predict.

Acknowledgements. The service charges for this open access publication have been covered by the Max Planck Society.

Topical Editor I. A. Daglis thanks two anonymous referees for their help in evaluating this paper.

References

Axford, W. I.: The Polar Wind and the Terrestrial Helium Budget, J. Geophys. Res., 73, 6855–6859, doi:10.1029/JA073i021p06855, 1968.

Barakat, A. R. and Schunk, R. W.: A three-dimensional model of the generalized polar wind, J. Geophys. Res. (Space Physics), 111, A12314, doi:10.1029/2006JA011662, 2006.

Baumjohann, W. and Haerendel, G.: Magnetospheric convection observed between 0600 and 2100 LT Solar wind and IMF dependence, J. Geophys. Res., 90, 6370–6378, 1985.

Baumjohann, W. and Paschmann, G.: Geometry of the near-earth plasma sheet, J. Geophys. Res., 95, 10707–10710, 1990.

Baumjohann, W., Haerendel, G., and Melzner, F.: Magnetospheric convection observed between 0600 and 2100 LT Variations with Kp, J. Geophys. Res., 90, 393–398, 1985.

Baumjohann, W., Nakamura, R., and Haerendel, G.: Dayside equatorial-plane convection and IMF sector structure, J. Geophys. Res., 91, 4557–4560, 1986.

Baumjohann, W., Paschmann, G., and Cattell, C. A.: Average plasma properties in the central plasma sheet, J. Geophys. Res., 94, 6597–6606, 1989.

Burton, R. K., McPherron, R. L., and Russell, C. T.: An empirical relationship between interplanetary conditions and D_{st}, J. Geophys. Res., 80, 4204–4214, 1975.

Caan, M. N., McPherron, R. L., and Russell, C. T.: Substorm and interplanetary magnetic field effects on the geomagnetic tail lobes, J. Geophys. Res., 80, 191–194, 1975.

Chappell, C. R., Moore, T. E., and Waite Jr., J. H.: The ionosphere as a fully adequate source of plasma for the earth's magnetosphere, J. Geophys. Res., 92, 5896–5910, doi:10.1029/JA092iA06p05896, 1987.

Comfort, R. H. and Horwitz, J. L.: Low energy ion pitch angle distributions observed on the dayside at geosynchronous altitudes, J. Geophys. Res., 86, 1621–1627, 1981.

Cowley, S. W. H., Morelli, J. P., and Lockwood, M.: Dependence of convection flows and particle precipitation in the high-latitude dayside ionosphere on the X and Y components of the interplanetary magnetic field, J. Geophys. Res., 96, 5557–5564, 1991.

Crooker, N. U.: An evolution of antiparallel merging, Geophys. Res. Lett., 13, 1063–1066, 1986.

Cully, C. M., Donovan, E. F., Yau, A. W., and Arkos, G. G.: Akebono/Suprathermal Mass Spectrometer observations of low-energy ion outflow: Dependence on magnetic activity and solar wind conditions, J. Geophys. Res. (Space Physics), 108, 1093, doi:10.1029/2001JA009200, 2003.

Cully, C. M., Ergun, R. E., and Eriksson, A. I.: Electrostatic structure around spacecraft in tenuous plasmas, J. Geophys. Res., 112, A09211, doi:10.1029/2007JA012269, 2007.

Dungey, J. R.: Interplanetary magnetic field and the auroral zones, Phys. Rev. Lett, 6, 47, 1961.

Engwall, E., Eriksson, A. I., André, M., Dandouras, I., Paschmann, G., Quinn, J., and Torkar, K.: Low-energy (order 10 eV) ion flow in the magnetotail lobes inferred from spacecraft wake observations, Geophys. Res. Lett., 33, 6110–6114, doi:10.1029/2005GL025179, 2006.

Engwall, E., Eriksson, A. I., Cully, C. M., André, M., Torbert, R., and Vaith, H.: Earth's ionospheric outflow dominated by hidden cold plasma, Nature Geosci., pp. 24–27, doi:10.1038/NGEO387, 2009a.

Engwall, E., Eriksson, A. I., Cully, C. M., André, M., Torbert, R., Vaith, H., and Puhl-Quinn, P.: Properties of ionospheric outflow examined from 5–19 RE in the Earth's magnetotail, Ann. Geophys., submitted, 2009b.

Eriksson, A. I., André, M., Klecker, B., Laakso, H., Lindqvist, P.-A., Mozer, F., Paschmann, G., Pedersen, A., Quinn, J., Torbert, R., Torkar, K., and Vaith, H.: Electric field measurements on Cluster: comparing the double-probe and electron drift techniques, Ann. Geophys., 24, 275–289, 2006, http://www.ann-geophys.net/24/275/2006/.

Escoubet, C. P., Schmidt, R., and Goldstein, M. L.: Cluster – Science and Mission Overview, Space Sci. Rev., 79, 11–32, 1997.

Förster, M., Paschmann, G., Haaland, S. E., Quinn, J. M., Torbert, R. B., Vaith, H., and Kletzing, C. A.: High-latitude plasma convection from Cluster EDI: variances and solar wind correlations, Ann. Geophys., 25, 1691–1707, 2007, http://www.ann-geophys.net/25/1691/2007/.

Förster, M., Haaland, S. E., Paschmann, G., Quinn, J. M., Torbert, R. B., Vaith, H., and Kletzing, C. A.: High-latitude plasma convection during Northward IMF as derived from in-situ magnetospheric Cluster EDI measurements, Ann. Geophys., 26, 2685–2700, 2008, http://www.ann-geophys.net/26/2685/2008/.

Gosling, J. T., Baker, D. N., Bame, S. J., Hones Jr., E. W., McComas, D. J., Zwickl, R. D., Slavin, J. A., Smith, E. J., and Tsurutani, B. T.: Plasma entry into the distant tail lobes – ISEE-3, Geophys. Res. Lett., 11, 1078–1081, 1984.

Gosling, J. T., Baker, D. N., Bame, S. J., Feldman, W. C., and Smith, E. J.: North-south and dawn-dusk plasma asymmetries in the distant tail lobes - ISEE 3, J. Geophys. Res., 90, 6354–6360, 1985.

Gustafsson, G., Bostrom, R., Holback, B.and Holmgren, G., Lundgren, A., Stasiewicz, K., Ahlen, L., Mozer, F. S., Pankow, D., Harvey, P., Berg, P., Ulrich, R., Pedersen, A., Schmidt, R., Butler, A., Fransen, A. W. C., Klinge, D., Thomsen, M., Falthammar, C.-G., Lindqvist, P.-A., Christenson, S., Holtet, J., Lybekk, B., Sten, T. A., Tanskanen, P., Lappalainen, K., and Wygant, J.: The Electric Field and Wave Experiment for the Cluster Mission, Space Sci. Rev., 79, 137–156, 1997.

Haaland, S. E., Paschmann, G., Förster, M., Quinn, J. M., Torbert, R. B., McIlwain, C. E., Vaith, H., Puhl-Quinn, P. A., and Kletzing, C. A.: High-latitude plasma convection from Cluster EDI measurements: method and IMF-dependence, Ann. Geophys., 25, 239–253, 2007, http://www.ann-geophys.net/25/239/2007/.

Haaland, S., Paschmann, G., Förster, M., Quinn, J., Torbert, R., Vaith, H., Puhl-Quinn, P., and Kletzing, C.: Plasma convection in the magnetotail lobes: statistical results from Cluster EDI measurements, Ann. Geophys., 26, 2371–2382, 2008, http://www.ann-geophys.net/26/2371/2008/.

Hasegawa, H., Fujimoto, M., Phan, T.-D., Rème, H., Balogh, A., Dunlop, M. W., Hashimoto, C., and TanDokoro, R.: Transport of solar wind into Earth's magnetosphere through rolled-up Kelvin-Helmholtz vortices, Nature, 430, 755–758, doi:10.1038/nature02799, 2004.

Hesse, M., Birn, J., and Hoffman, R. A.: On the mapping of ionospheric convection into the magnetosphere, J. Geophys. Res., 102, 9543–9552, doi:10.1029/96JA03999, 1997.

Huang, C. Y. and Frank, L. A.: A statistical survey of the central plasma sheet, J. Geophys. Res., 99, 83–95, 1994.

Huddleston, M. M., Chappell, C. R., Delcourt, D. C., Moore, T. E., Giles, B. L., and Chandler, M. O.: An examination of the process and magnitude of ionospheric plasma supply to the magnetosphere, J. Geophys. Res. (Space Physics), 110, A12202, doi:10.1029/2004JA010401, 2005.

Imber, S. M., Milan, S. E., and Hubert, B.: The auroral and ionospheric flow signatures of dual lobe reconnection, Ann. Geophys., 24, 3115–3129, 2006, http://www.ann-geophys.net/24/3115/2006/.

Imber, S. M., Milan, S. E., and Hubert, B.: Observations of significant flux closure by dual lobe reconnection, Ann. Geophys., 25, 1617–1627, 2007, http://www.ann-geophys.net/25/1617/2007/.

Johnstone, A. D., Alsop, C., Burge, S., Carter, P. J., Coates, A. J., Coker, A. J., Fazakerley, A. N., Grande, M., Gowen, R. A., Gurgiolo, C., Hancock, B. K., Narheim, B., Preece, A., Sheather, P. H., Winningham, J. D., and Woodliffe, R. D.: Peace: a Plasma Electron and Current Experiment, Space Sci. Rev., 79, 351–398, 1997.

Lennartsson, O. W.: Tail lobe ion composition at energies of 0.1 to 16 keV/e: Evidence for mass-dependent density gradients, J. Geophys. Res., 99, 2387–2401, 1994.

Lennartsson, O. W., Collin, H. L., and Peterson, W. K.: Solar wind control of Earth's H^+ and O^+ outflow rates in the 15-eV to 33-keV energy range, J. Geophys. Res. (Space Physics), 109, A12212, doi:10.1029/2004JA010690, 2004.

Lennartsson, W. and Sharp, R. D.: A comparison of the 0.1–17 keV/e ion composition in the near equatorial magnetosphere between quiet and disturbed conditions, J. Geophys. Res., 87, 6109–6120, 1982.

Lockwood, M., Waite Jr., J. H., Moore, T. E., Chappell, C. R., and Chandler, M. O.: The cleft ion fountain, J. Geophys. Res., 90, 9736–9748, doi:10.1029/JA090iA10p09736, 1985a.

Lockwood, M., Waite, Jr., J. H., Moore, T. E., Chappell, C. R., and Johnson, J. F. E.: A new source of suprathermal O(+) ions near the dayside polar cap boundary, J. Geophys. Res., 90, 4099–4116, doi:10.1029/JA090iA05p04099, 1985b.

Mailyan, B., Munteanu, C., and Haaland, S.: What is the best method to calculate the solar wind propagation delay?, Ann. Geophys., 26, 2383–2394, 2008, http://www.ann-geophys.net/26/2383/2008/.

Matsui, H., Quinn, J. M., Torbert, R. B., Jordanova, V. K., Puhl-Quinn, P. A., and Paschmann, G.: IMF B_Y and the seasonal dependences of the electric field in the inner magnetosphere, Ann. Geophys., 23, 2671–2678, 2005, http://www.ann-geophys.net/23/2671/2005/.

Maynard, N. C., Sojka, J. J., Schunk, R. W., Heppner, J. P., and Brace, L. H.: A Test of convection models for IMF B_z North, Planet. Space Sci., 38, 1077–1089, doi:10.1016/0032-0633(90)90017-K, 1990.

Maynard, N. C., Denig, W. F., and Burke, W. J.: Mapping ionospheric convection patterns to the magnetosphere, J. Geophys. Res., 100, 1713–1721, 1995.

Noda, H., Baumjohann, W., Nakamura, R., Torkar, K., Paschmann, G., Vaith, H., Puhl-Quinn, P., Förster, M., Torbert, R., and Quinn, J. M.: Tail lobe convection observed by Cluster/EDI, J. Geophys. Res., 108, 1288, doi:10.1029/2002JA009669, 2003.

O'Brien, T. P. and McPherron, R. L.: An empirical phase space

analysis of ring current dynamics: Solar wind control of injection and decay, J. Geophys. Res., 105, 7707–7720, doi:10.1029/1998JA000437, 2000.

Øieroset, M., Phan, T. D., Angelopoulos, V., Eastwood, J. P., McFadden, J., Larson, D., Carlson, C. W., Glassmeier, K.-H., Fujimoto, M., and Raeder, J.: THEMIS multi-spacecraft observations of magnetosheath plasma penetration deep into the dayside low-latitude magnetosphere for northward and strong B_y IMF, Geophys. Res. Lett., 35, 17–22, doi:10.1029/2008GL033661, 2008.

Paschmann, G., Melzner, F., Frenzel, R., Vaith, H., Parigger, P., Pagel, U., Bauer, O. H., Haerendel, G., Baumjohann, W., Scopke, N., Torbert, R. B., Briggs, B., Chan, J., Lynch, K., Morey, K., Quinn, J. M., Simpson, D., Young, C., McIlwain, C. E., Fillius, W., Kerr, S. S., Mahieu, R., and Whipple, E. C.: The Electron Drift Instrument for Cluster, Space Sci. Rev., 79, 233–269, 1997.

Paschmann, G., Quinn, J. M., Torbert, R. B., Vaith, H., McIlwain, C. E., Haerendel, G., Bauer, O. H., Bauer, T., Baumjohann, W., Fillius, W., Förster, M., Frey, S., Georgescu, E., Kerr, S. S., Kletzing, C. A., Matsui, H., Puhl-Quinn, P., and Whipple, E. C.: The Electron Drift Instrument on Cluster: overview of first results, Ann. Geophys., 19, 1273–1288, 2001, http://www.ann-geophys.net/19/1273/2001/.

Pedersen, A., Mozer, F., and Gustafsson, G.: Electric Field Measurements in a Tenuous Plasma with Spherical Double Probes, in: Measurement Techniques in Space Plasmas – Fields, edited by: Pfaff, R. F., Borovsky, J. E., and Young, D. T., pp. 1–12, 1998.

Pedersen, A., Lybekk, B., André, M., Eriksson, A., Masson, A., Mozer, F. S., Lindqvist, P.-A., Décréau, P. M. E., Dandouras, I., Sauvaud, J.-A., Fazakerley, A., Taylor, M., Paschmann, G., Svenes, K. R., Torkar, K., and Whipple, E.: Electron density estimations derived from spacecraft potential measurements on Cluster in tenuous plasma regions, J. Geophys. Res., 113, A07S33, doi:10.1029/2007JA012636, 2008.

Pulkkinen, T. I. and Tsyganenko, N. A.: Testing the accuracy of magnetospheric model field line mapping, J. Geophys. Res., 101, 27431–27442, doi:10.1029/96JA02489, 1996.

Quinn, J. M., Paschmann, G., Torbert, R. B., Vaith, H., McIlwain, C. E., Haerendel, G., Bauer, O., Bauer, T. M., Baumjohann, W., Fillius, W., Foerster, M., Frey, S., Georgescu, E., Kerr, S. S., Kletzing, C. A., Matsui, H., Puhl-Quinn, P., and Whipple, E. C.: Cluster EDI convection measurements across the high-latitude plasma sheet boundary at midnight, Ann. Geophys., 19, 1669–1681, 2001, http://www.ann-geophys.net/19/1669/2001/.

Rème, H., Aoustin, C., Bosqued, J. M., Dandouras, I., Lavraud, B., Sauvaud, J. A., Barthe, A., Bouyssou, J., Camus, Th., Coeur-Joly, O., Cros, A., Cuvilo, J., Ducay, F., Garbarowitz, Y., Medale, J. L., Penou, E., Perrier, H., Romefort, D., Rouzaud, J., Vallat, C., Alcaydé, D., Jacquey, C., Mazelle, C., d'Uston, C., Mbius, E., Kistler, L. M., Crocker, K., Granoff, M., Mouikis, C., Popecki, M., Vosbury, M., Klecker, B., Hovestadt, D., Kucharek, H., Kuenneth, E., Paschmann, G., Scholer, M., Sckopke, N., Seidenschwang, E., Carlson, C. W., Curtis, D. W., Ingraham, C., Lin, R. P., McFadden, J. P., Parks, G. K., Phan, T., Formisano, V., Amata, E., Bavassano-Cattaneo, M. B., Baldetti, P., Bruno, R., Chionchio, G., Di Lellis, A., Marcucci, M. F., Pallocchia, G., Korth, A., Daly, P. W., Graeve, B., Rosenbauer, H., Vasyliunas, V., McCarthy, M., Wilber, M., Eliasson, L., Lundin, R., Olsen, S., Shelley, E. G., Fuselier, S., Ghielmetti, A. G., Lennartsson, W., Escoubet, C. P., Balsiger, H., Friedel, R., Cao, J.-B., Kovrazhkin, R. A., Papamastorakis, I., Pellat, R., Scudder, J., and Sonnerup, B.: First multispacecraft ion measurements in and near the Earth's magnetosphere with the identical Cluster ion spectrometry (CIS) experiment, Ann. Geophys., 19, 1303–1354, 2001, http://www.ann-geophys.net/19/1303/2001/.

Rosenbauer, H., Gruenwaldt, H., Montgomery, M. D., Paschmann, G., and Sckopke, N.: Heos 2 plasma observations in the distant polar magnetosphere – The plasma mantle, J. Geophys. Res., 80, 2723–2737, 1975.

Ruohoniemi, J. M. and Baker, K. B.: Large-scale imaging of high-latitude convection with Super Dual Auroral Radar Network HF radar observations, J. Geophys. Res., 103, 20797–20812, 1998.

Russell, C. T., Zhou, X. W., Chi, P. J., Kawano, H., Moore, T. E., Peterson, W. K., Cladis, J. B., and Singer, H. J.: Sudden compression of the outer magnetosphere associated with an ionospheric mass ejection, Geophys. Res. Lett., 26, 2343–2346, doi:10.1029/1999GL900455, 1999.

Sandholt, P. E., Farrugia, C. J., Cowley, S. W. H., Denig, W. F., Lester, M., Moen, J., and Lybekk, B.: Capture of magnetosheath plasma by the magnetosphere during northward IMF, Geophys. Res. Lett., 26, 2833–2836, doi:10.1029/1999GL900600, 1999.

Schwartz, S. J.: Shock and Discontinuity Normals, Mach Numbers, and Related Parameters, in: Analysis Methods for Multi-Spacecraft Data, edited by: Paschmann, G. and Daly, P. W., ISSI SR-001, p. 249, ESA Publications Division, 1998.

Shue, J.-H., Chao, J. K., Fu, H. C., Russell, C. T., Song, P., Khurana, K. K., and Singer, H. J.: A new functional form to study the solar wind control of the magnetopause size and shape, J. Geophys. Res., 102, 9497–9512, doi:10.1029/97JA00196, 1997.

Smart, D. F. and Shea, M. A.: A comparison of the tsyganenko model predicted and measured geomagnetic cutoff latitudes, Adv. Space Res., 28, 1733–1738, 2001.

Strangeway, R. J., Russell, C. T., Carlson, C. W., McFadden, J. P., Ergun, R. E., Temerin, M., Klumpar, D. M., Peterson, W. K., and Moore, T. E.: Cusp field-aligned currents and ion outflows, J. Geophys. Res., 105, 21129–21142, doi:10.1029/2000JA900032, 2000.

Strangeway, R. J., Ergun, R. E., Su, Y.-J., Carlson, C. W., and Elphic, R. C.: Factors controlling ionospheric outflows as observed at intermediate altitudes, J. Geophys. Res., 110, A03221, doi:10.1029/2004JA010829, 2005.

Svenes, K. R., Lybekk, B., Pedersen, A., and Haaland, S.: Cluster observations of near-Earth magnetospheric lobe plasma densities – a statistical study, Ann. Geophys., 26, 2845–2852, 2008, http://www.ann-geophys.net/26/2845/2008/.

Taylor, M. G. G. T., Lavraud, B., Escoubet, C. P., Milan, S. E., Nykyri, K., Dunlop, M. W., Davies, J. A., Friedel, R. H. W., Frey, H., Bogdanova, Y. V., Åsnes, A., Laakso, H., Trávnıĉek, P., Masson, A., Opgenoorth, H., Vallat, C., Fazakerley, A. N., Lahiff, A. D., Owen, C. J., Pitout, F., Pu, Z., Shen, C., Zong, Q. G., Rème, H., Scudder, J., and Zhang, T. L.: The plasma sheet and boundary layers under northward IMF: A multi-point and multi-instrument perspective, Adv. Space Res., 41, 1619–1629, doi:10.1016/j.asr.2007.10.013, 2008.

Torkar, K., Riedler, W., Escoubet, C. P., Fehringer, M., Schmidt, R., Grard, R. J. L., Arends, H., Rüdenauer, F., Steiger, W., Narheim,

B. T., Svenes, K., Torbert, R., Andr, M., Fazakerley, A., Goldstein, R., Olsen, R. C., Pedersen, A., Whipple, E., and Zhao, H.: Active spacecraft potential control for Cluster – implementation and first results, Ann. Geophys., 19, 1289–1302, 2001, http://www.ann-geophys.net/19/1289/2001/.

Treumann, R. A., Labelle, J., and Bauer, T. M.: Diffusion Processes: An Observational Perspective, in: Physics of the Magnetopause, pp. 331–341, American Geophysical Union, 1995.

Tsyganenko, N. A.: A model of the near magnetosphere with a dawn-dusk asymmetry 1. Mathematical structure, J. Geophys. Res., 107, 1179, doi:10.1029/2001JA000219, 2002a.

Tsyganenko, N. A.: A model of the near magnetosphere with a dawn-dusk asymmetry 2. Parameterization and fitting to observations, J. Geophys. Res., 107, 1176, doi:10.1029/2001JA000220, 2002b.

Vaisberg, O. L., Avanov, L. A., Burch, J. L., and Waite, J. H.: Measurements of plasma in the magnetospheric tail lobes, Adv. Space Res., 18, 63–67, 1996.

Weimer, D. R. and King, J. H.: Improved calculations of interplanetary magnetic field phase front angles and propagation time delays, J. Geophys. Res., 113, A01105, doi:10.1029/2007JA012452, 2008.

Weimer, D. R., Ober, D. M., Maynard, N. C., Collier, M. R., McComas, D. J., Ness, N. F., Smith, C. W., and Watermann, J.: Predicting interplanetary magnetic field (IMF) propagation delay times using the minimum variance technique, J. Geophys. Res., 108, 1026, doi:10.1029/2002JA009405, 2003.

Wilken, B., Goertz, C. K., Baker, D. N., Higbie, P. R., and Fritz, T. A.: The SSC on July 29, 1977 and its propagation within the magnetosphere, J. Geophys. Res., 87, 5901–5910, doi:10.1029/JA087iA08p05901, 1982.

Wing, S. and Newell, P. T.: 2D plasma sheet ion density and temperature profiles for northward and southward IMF, Geophys. Res. Lett., 29, 21–1, doi:10.1029/2001GL013950, 2002.

Woodfield, E. E., Dunlop, M. W., Holme, R., Davies, J. A., and Hapgood, M. A.: A comparison of Cluster magnetic data with the Tsyganenko 2001 model, J. Geophys. Res., 112, 6248–6259, doi:10.1029/2006JA012217, 2007.

Yau, A. W. and Andre, M.: Sources of Ion Outflow in the High Latitude Ionosphere, Space Sci. Rev., 80, 1–25, doi:10.1023/A:1004947203046, 1997.

Young, D. T., Balsiger, H., and Geiss, J.: Correlations of magnetospheric ion composition with geomagnetic and solar activity, J. Geophys. Res., 87, 9077–9096, 1982.